



Communication: Theoretical exploration of Au⁺⁺H₂, D₂, and HD reactive collisions

Anaís Dorta-Urra, Alexandre Zanchet, Octavio Roncero, Alfredo Aguado, and P. B. Armentrout

Citation: *J. Chem. Phys.* **135**, 091102 (2011); doi: 10.1063/1.3635772

View online: <http://dx.doi.org/10.1063/1.3635772>

View Table of Contents: <http://jcp.aip.org/resource/1/JCPSA6/v135/i9>

Published by the [American Institute of Physics](http://www.aip.org).

Additional information on *J. Chem. Phys.*

Journal Homepage: <http://jcp.aip.org/>

Journal Information: http://jcp.aip.org/about/about_the_journal

Top downloads: http://jcp.aip.org/features/most_downloaded

Information for Authors: <http://jcp.aip.org/authors>

ADVERTISEMENT



AIPAdvances

Submit Now

Explore AIP's new
open-access journal

- Article-level metrics now available
- Join the conversation! Rate & comment on articles

Communication: Theoretical exploration of $\text{Au}^+ + \text{H}_2$, D_2 , and HD reactive collisions

Anaís Dorta-Urra,¹ Alexandre Zanchet,¹ Octavio Roncero,^{1,a)} Alfredo Aguado,² and P. B. Armentrout³

¹ Unidad Asociada UAM-CSIC, Instituto de Física Fundamental, C.S.I.C. Serrano 123, 28006 Madrid, Spain

² Unidad Asociada UAM-CSIC, Departamento de Química Física, Facultad de Ciencias C–XIV, Universidad Autónoma de Madrid, 28049 Madrid, Spain

³ Department of Chemistry, University of Utah, 315 S. 1400 E. Rm 2020, Salt Lake City, Utah 84112, USA

(Received 15 July 2011; accepted 17 August 2011; published online 6 September 2011; publisher error corrected 12 September 2011)

A quasi-classical study of the endoergic $\text{Au}^+(^1S) + \text{H}_2(X^1\Sigma_g^+) \rightarrow \text{AuH}^+(^2\Sigma^+) + \text{H}(^2S)$ reaction, and isotopic variants, is performed to compare with recent experimental results [F. Li, C. S. Hinton, M. Citir, F. Liu, and P. B. Armentrout, *J. Chem. Phys.* **134**, 024310 (2011)]. For this purpose, a new global potential energy surface has been developed based on multi-reference configuration interaction *ab initio* calculations. The quasi-classical trajectory results show a very good agreement with the experiments, showing the same trends for the different isotopic variants of the hydrogen molecule. It is also found that the total dissociation into three fragments, $\text{Au}^+ + \text{H} + \text{H}$, is the dominant reaction channel for energies above the H_2 dissociation energy. This results from a well in the entrance channel of the potential energy surface, which enhances the probability of H–Au–H insertion. © 2011 American Institute of Physics. [doi:10.1063/1.3635772]

Bond first evaluated gold and gold alloy catalysts and their activity for hydrogenation.¹ Subsequent work focused on the reactivity of gold.^{2,3} In 1987, Haruta *et al.*⁴ observed experimentally that gold nanoparticles catalyze the oxidation of CO at low temperatures. After this, it has been shown that gold becomes active for many reactions when stabilized in the form of nanoparticles, even more than platinum group metals (PGMs) (Ref. 5) in selective oxidation reactions.

Intense work has focused on the reactivity of neutral and charged gold clusters, isolated as well as supported on different substrates.⁶ Reactivity is intimately connected to the electronic structure and geometry of the cluster, and gold nanoparticles present a very interesting variety of forms,⁷ such as nanowires,^{8,9} planar (2d) clusters,^{10–12} and cages.^{13,14} The peculiar reactivity of gold is attributed to important relativistic effects, which makes the $6s$ and $5d$ orbitals become closer in energy than in other coinage atoms allowing efficient sd hybridization.¹⁵

The mechanism of molecular hydrogen dissociation on small models of gold chains has been studied, showing minimum energy paths (MEP) with no barrier.¹⁶ Recently, the effect of the size, geometry, and charge of small planar gold clusters on the dissociation barrier of H_2 has been studied.¹⁷ It was found that H_2 is preferentially attached to sites with positive charge densities. The presence of such potential wells was found to be a necessary requirement for reaction to occur. This factor favors the reactivity of cationic clusters. However, a second requirement involves curve crossings with excited electronic states, which determines the height of the H_2 dis-

sociation barrier. This crossing allows those anionic species with positive charge density sites to present lower barriers than neutral or cationic species.

These charge and curve crossing effects can be studied in more detail in the case of one gold atom. This allows the accurate determination of the potential energy surfaces (PES) of the ground and excited electronic states, and the comparison with detailed gas-phase experimental results.^{18–20} Recently, it has been shown that a single neutral gold atom in the ground electronic state presents very high barriers for H_2 dissociation.²¹ The PES of the ground state presents a potential well high in energy, considered as a precursor of the chemisorption well appearing in gold nanoparticles and originating from several curve crossings. Particularly interesting is the recent experimental study²² of the $\text{Au}^+ + \text{H}_2 \rightarrow \text{AuH}^+ + \text{H}$ reaction, and its isotopologues, HD and D_2 . This system provides a good benchmark to analyze the effect of the positive charge in this reaction from a theoretical point of view. This work presents a detailed study of this reaction by developing a global PES based on highly accurate *ab initio* points and determining the cross sections for the different reaction channels using quasi-classical trajectory (QCT) calculations.

The *ab initio* calculations are performed with the MOLPRO suite of programs²³ using same methods (MC-SCF/ic-MRCI) and basis set²⁴ than in our previous work on the neutral AuH_2 system.²¹ The 0 K dissociation energies of H_2 and AuH^+ obtained are $D_0 = 4.44$ and 1.79 eV, respectively, including zero-point energy corrections. These values are very similar to theoretical results summarized previously in Ref. 22 of 4.51 for H_2 and in the range from 1.26 to 2.08 eV for AuH^+ . The experimental values are 4.478 eV

^{a)} Author to whom correspondence should be addressed. Electronic mail: octavio.roncero@csic.es.

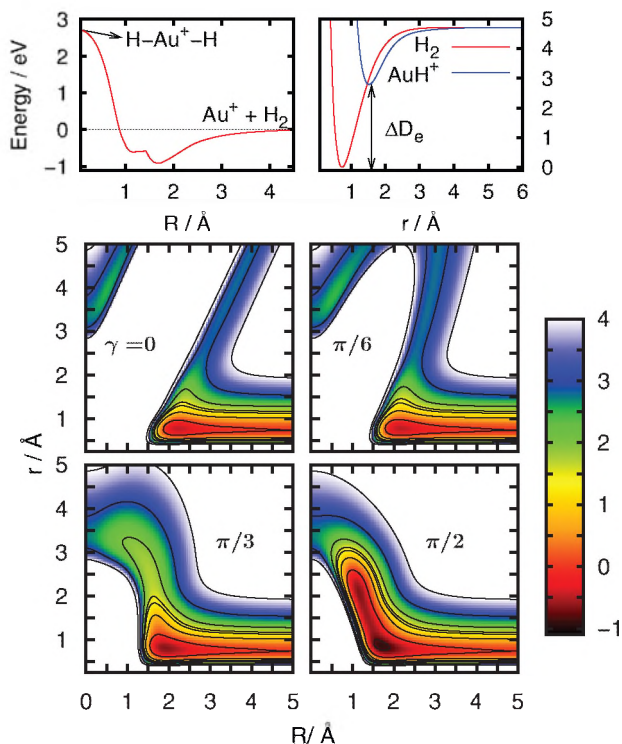


FIG. 1. MEP (left, top panel) in eV for the PES of the $^1A'$ ground state of AuH_2^+ . Diatomic energy curves for H_2 and AuH^+ in eV (right, top panel). Lower panels: contour plots of the PES as a function of the two Jacobi distances, r and R , for the angles $\gamma = 0, \pi/6, \pi/3$, and $\pi/2$. The contours correspond to $-0.8, 0, 0.8, 1.3, 1.5, 2, 3, 4$ eV.

for H_2 and 2.13 ± 0.11 for AuH^+ ,²² where the latter value is slightly higher than the lower limit obtained from reaction with CH_4 ($>1.94 \pm 0.08$) eV.²⁵ We can then conclude that the present calculations are of sufficient accuracy to describe the PES. About 9043 *ab initio* points have been calculated in a grid in Jacobi reactants coordinates, as described previously.²¹ The *ab initio* icMRCI+Q energies for the ground electronic state of AuH_2^+ , $^1A'$, has been fitted using the GFIT3C procedure.^{26,27} The overall rms error of the fitted PES is 0.06 eV.

An approximate MEP is shown in the left top panel of Fig. 1 as a function of the distance, R , between Au^+ and the center of mass of H_2 , in which the H–H distance, r , corresponds to that of the minimum energy, and the angle, γ , between \mathbf{r} and \mathbf{R} vectors is set equal to $\pi/2$. The PES shows a well of ≈ 0.91 eV in the entrance channel, which is more clearly displayed in the contour plots of the PES shown in the lower panels of Fig. 1 and is very similar to that reported in Ref. 22 of 0.87 eV. Also, in the right top panel, the potential for the two diatomic species is shown, showing the large difference of dissociation energies, ΔD_e , equal to the endothermicity of the $\text{Au}^+ + \text{H}_2 \rightarrow \text{AuH}^+ + \text{H}$ reaction, when the zero-point energy of the diatomic fragments are not taken into account.

The well of the entrance channel has an important contribution from the charge-quadrupole interaction between Au^+ and H_2 and does not exist in neutral AuH_2 which only presents a H–Au–H insertion well.²¹ Small planar gold clusters also present a well in the entrance channel at sites with a deficit

of electronic density, associated with local positive charges.¹⁷ Such sites can also occur in neutral and anionic systems, as a consequence of the polarization of the electronic density in gold clusters.

The characteristics of the insertion well with charge of the AuH_2 system can be understood by considering the low energy orbitals. The $6a_1$ orbital, which is largely $\text{Au}(6s)$, is the LUMO in Au^+-H_2 , whereas $\text{Au}+\text{H}_2$ and Au^-+H_2 have 1 and 2 electrons in the $6a_1$ orbital, respectively. The energy of this orbital crosses with that of the $3b_2$ orbital, largely $\text{H}_2(\sigma_u)$ with contributions from $\text{Au}(6p_x)$, when the gold atom approaches H_2 . At the crossing, which is avoided in C_s symmetry, the neutral and anionic systems show a barrier. After this barrier, these electrons move to the $3b_2$ orbital, whose energy decreases as R distance decreases. The stabilization of the anion is larger than the neutral, with 2 electrons in this $3b_2$ orbital, leading to a deeper H–Au–H insertion well, ≈ 0.25 eV below the Au^-+H_2 asymptote. For the cation, the well in the entrance channel extends to something close to an insertion well visible near $R = 1$ Å and $r = 2$ Å that can be seen in Fig. 1. The H–Au–H angle in the entrance well is 27.2° in very good agreement with that given in Ref. 22. These plots also show that the linear configuration with Au^+ in between the two H atoms is not stable. In the neutral, the situation is somewhat intermediate: the well does not appear in the entrance channel, the linear H–Au–H species is not stable, but a shallow insertion well having a bent geometry appears. It could be argued that this situation is a result of the different occupation numbers of the $6a_1/3b_2$ orbital, unoccupied for the cation and with 1 and 2 electrons in the case of the neutral and anion.

The $\text{Au}^+ + \text{H}_2(v = 0, j = 0) \rightarrow \text{AuH}^+ + \text{H}$ reaction, and deuterated variants, are studied using the QCT method because the reaction is very endoergic, such that high translational energies are required for reaction to occur. The initial conditions are determined using a standard Monte Carlo sampling method introduced by Karplus *et al.*²⁸ The impact parameter is initially set in the interval of 0–1.9 Å, and the distance between center of mass of reactants is set to $R = 10$ Å. The 500 000 trajectories are propagated for each collision energy, from 2.5 up to 8.5 eV, in steps of 0.1 eV. The trajectories are stopped when the distance between any pair of atoms is larger than 20 Å. The products fragments are then assigned as H_2 , AuH^+ , and AuD^+ diatomic fragments, or to total dissociation, $\text{Au}^+ + \text{H} + \text{H}$. This is performed by first analyzing if the distance and energy for any pair of atoms are below a given threshold, typically 10 a.u. of distance and the corresponding diatomic dissociation energy, respectively. Once the final products are assigned, the probabilities and cross sections for each event are obtained.

The cross sections obtained for each of the isotopic variants are shown in Fig. 2 and compared with the experimental ones of Ref. 22 (obtained under single collision conditions) in absolute units. The agreement is good, but the theoretical cross sections show a threshold at higher energy, such that they are narrower as well. This reflects the fact that the theoretical threshold energy of 2.65 eV is 0.3 eV above the experimental one.²² Furthermore, experimental results are broadened by several effects. Among them, the kinetic energy distributions of the reactants are the most important

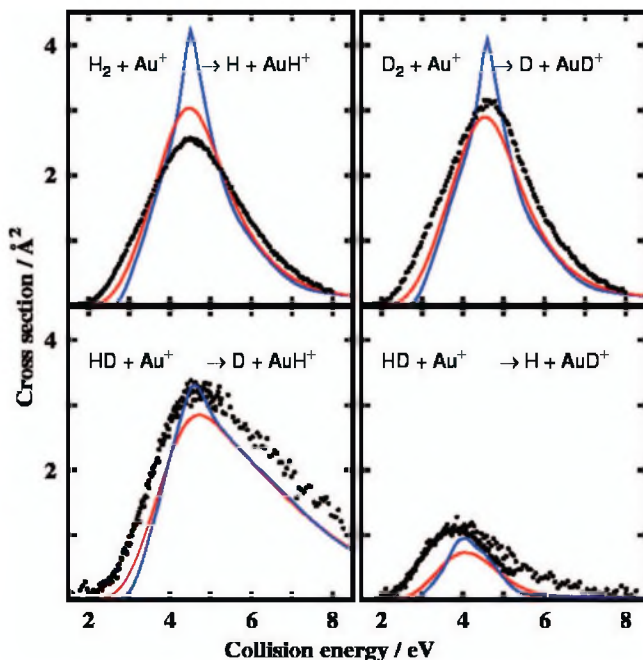


FIG. 2. Reaction cross sections for the $\text{Au}^+ + \text{H}_2 \rightarrow \text{AuH}^+ + \text{H}$ collisions (and isotopic variants), as a function of collision energy. The experimental data (Ref. 22) are represented by solid circles. Blue lines correspond to QCT calculations at fixed energies and red lines to the convolutions of the QCT results over the kinetic and internal energy distributions of the reactants.

and possible to model experimentally. The distribution of Au^+ kinetic energy is nearly Gaussian and has a typical full width at half maximum between 0.3 and 1.0 eV in the laboratory frame, which is <0.02 eV in the center-of-mass frame.²² Likewise, although the neutral reactants can have energy from rotations, this is on the order of $k_B T$ at 300 K or 0.03 eV. The most significant contribution to the experimental broadening is the thermal motion of the light neutral reagents or Doppler broadening.²⁹ We account for this by explicitly convoluting the QCT results with the kinetic and internal energy distributions of the reactants using the data analysis program CRUNCH.³⁰ These convoluted cross sections are shown as red lines in Fig. 2. The agreement between experiment and simulations improves, both with respect to the maximum magnitude of the cross section and the apparent energy threshold. As noted above, the remaining differences may be attributed to errors in the determination of the dissociation energies of the diatoms, see Fig. 1.

This energy threshold difference can be approximately accounted for using a simple line-of-centers like form, $\sigma(E) = \sigma_0 (E - E_0)^n / E$, coupled with a simple model previously described for the probability of further dissociation of the AuH^+ (AuD^+) products to $\text{Au}^+ + \text{H}$ (D).³⁰ The best reproduction of the QCT results yields values of the parameter n very close to those found to reproduce the experimental results, namely, $n = 1.5 - 1.6$.²² Using this model, with $n = 1.5 - 1.6$ and the experimental E_0 value (0.3 eV lower than the *ab initio* one), together with the convolution procedure described above, the results reproduced the experimental points very well. In this comparison, a difference in the scaling factor (σ_0) of factors of 0.70 and 0.82 is needed to reproduce the absolute

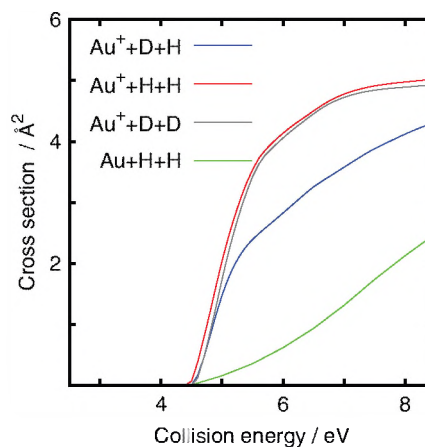


FIG. 3. Reaction cross sections obtained for total fragmentation channel, $\text{Au}^+ + \text{H} + \text{H}$ (and isotopic variants) in the $\text{Au}^+ + \text{H}_2$ collisions. The cross section obtained for the neutral $\text{Au} + \text{H}_2$ collisions is also shown for comparison.

experimental results for H_2 and D_2 , respectively. The difference between these two scaling factors is attributed to the experimental results, because the QCT cross sections for the two systems are essentially of the same magnitude. As discussed in the experimental paper,²² the differences are just within the overall 20% uncertainty intrinsic to the absolute cross section measurements.

For the $\text{Au}^+ + \text{HD}$ reaction, the agreement in the branching ratio between the two products channels is again very good. It is clearly more favorable to form AuH^+ than AuD^+ fragments. This situation is typical in atomic ion reactions with HD and has been explained in detail in Refs. 20 and 31. For electronic configurations having an empty valence s orbital, the relative yields of MH^+ versus MD^+ products is controlled by angular momentum conservation, which favors formation of the product channel having the larger reduced mass, $\text{AuH}^+ + \text{D}$, compared to that of $\text{AuD}^+ + \text{H}$. In the present simulation, the PES cannot distinguish between H and D atoms, in agreement with the idea that the branching ratio is controlled by a dynamical effect.

Above the threshold for total dissociation, ≈ 4.5 eV, it is possible to fragment the whole system into three atoms. The simulated cross section for the $\text{Au}^+ + \text{H}_2 \rightarrow \text{Au}^+ + \text{H} + \text{H}$ process and isotopic variants are shown in Fig. 3. In all cases, the total fragmentation cross section increases very rapidly above this threshold and becomes dominant for energies above 5.5 eV, with a probability $>50\%$ for impact parameters $b_{\text{max}} < 1.8$ Å considered here for reactive collisions. In the case of $\text{Au}^+ + \text{HD}$, the total fragmentation cross section increases more slowly, the AuH^+ channel becoming more probable as can be seen from cross sections shown in Fig. 2. Because the PES is the same for all three systems, the only thing that changes is the mass, specifically the D atom neutral product can carry away more energy in translation than the lighter H atom product.

One final question to address is why the total fragmentation process is so favorable. H_2 is small and tightly bound, such that it seems improbable that a big heavy atom such as gold could break it efficiently. *A priori*, one might expect that a collision is more likely to transfer the kinetic energy

to the H₂ as a whole, without breaking it. The reason for the efficient dissociation can be understood from the presence of the potential well in the entrance channel. This well is deeper for T-shaped configurations, such that the H₂ reorients when Au⁺ atom arrives. Thus, Au⁺ directly collides with the center-of-mass of the H₂ and, at the high energies considered, allows the system to arrive at the H–Au⁺–H insertion configuration, in which H₂ is already dissociated.

To emphasize this relationship, the same kind of calculations have been performed for neutral Au+H₂, whose PES does not contain the entrance well, but only the insertion H–Au–H well, as described previously.²¹ In this case, as shown in Fig. 3, the total fragmentation mechanism becomes less favorable, and its cross section increases more slowly with energy. A similar situation holds for the reaction probability, which increases continuously up to 40% for 8.5 eV. Because this system also contains a deeper insertion well, it could conceivably result in a higher total fragmentation cross section. However, this is not the case, indicating that the stronger interaction in the entrance channel for the Au⁺ case leads to the more efficient dissociation.

A.D.-U. acknowledges a JAE fellowship supported by CSIC. This work is supported by Comunidad Autónoma de Madrid, Grant No. S-2009/MAT/I467, and by Ministerio de Ciencia e Innovación, Grant Nos. CSD2009-00038 and FIS2010-18132. The calculations have been performed at CESGA and IFF computing centers. P.B.A. thanks the National Science Foundation for support.

¹G. C. Bond, *Gold Bull.* **5**, 11 (1972).

²J. Figar and W. Haidiger, *Gold Bull.* **7**, 100 (1974).

³D. I. Bradshaw, R. B. Moyes, and P. B. Weils, *J. Chem. Soc., Chem. Commun.* **1975**, 137.

⁴M. Haruta, T. Kobayashi, H. Sano, and N. Yamada, *Chem. Lett.* **16**, 405 (1987).

⁵G. C. Bond, *Gold Bull.* **41**, 235 (2008).

⁶R. Coquet, K. L. Howard, and D. J. Willock, *Chem. Soc. Rev.* **37**, 2046 (2008).

⁷H. Häkkinen, *Chem. Soc. Rev.* **37**, 1847 (2008).

⁸A. I. Yanson, G. R. Bollinger, H. E. van den Brom, N. Agrait, and J. M. van Ruitenbeek, *Nature (London)* **395**, 783 (1998).

⁹H. Häkkinen, R. N. Barnett, and U. Landman, *J. Phys. Chem. B* **103**, 8814 (1999).

¹⁰H. Häkkinen and U. Landman, *Phys. Rev. B* **62**, R2287 (2000).

¹¹S. Gilb, P. Weis, F. Furche, R. Ahlrichs, and M. M. Kappes, *J. Chem. Phys.* **116**, 4094 (2002).

¹²A. Lechtken, C. Neiss, M. M. Kappes, and D. Schooss, *Phys. Chem. Chem. Phys.* **11**, 4344 (2009).

¹³R. B. King, Z. Chen, and P. v. R. Schleyer, *Inorg. Chem.* **43**, 4564 (2004).

¹⁴S. Bulusu and X. C. Zeng, *J. Chem. Phys.* **125**, 154303 (2006).

¹⁵H. Häkkinen, M. Moseler, and U. Landman, *Phys. Rev. Lett.* **89**, 033401 (2002).

¹⁶A. Zanchet, A. Dorta-Urra, O. Roncero, F. Flores, C. Tablero, M. Paniagua, and A. Aguado, *Phys. Chem. Chem. Phys.* **11**, 10122 (2009).

¹⁷A. Zanchet, A. Dorta-Urra, A. Aguado, and O. Roncero, *J. Phys. Chem. C* **115**, 47 (2011).

¹⁸M. Ishida, R. Yamashiro, Y. Matsumoto, and K. Honma, *J. Chem. Phys.* **124**, 204316 (2006).

¹⁹J. J. Schrodren, H. F. Davis, and C. A. Bayse, *J. Phys. Chem. A* **111**, 11421 (2007).

²⁰P. B. Armentrout, *Int. Rev. Phys. Chem.* **9**, 115 (1990).

²¹A. Zanchet, O. Roncero, S. Omar, M. Paniagua, and A. Aguado, *J. Chem. Phys.* **132**, 034301 (2010).

²²F. Li, C. S. Hinton, M. Citir, F. Liu, and P. B. Armentrout, *J. Chem. Phys.* **134**, 024310 (2011).

²³MOLPRO, a package of *ab initio* programs designed by H.-J. Werner and P. J. Knowles, version 2006.1, R. D. Amos, A. Bernhardsson, A. Berning *et al.*

²⁴D. Figgen, G. Rauhut, M. Dolg, and H. Stoll, *Chem. Phys.* **311**, 227 (2005).

²⁵P. B. Armentrout and F.-X. Li, *J. Chem. Phys.* **125**, 133114 (2006).

²⁶A. Aguado and M. Paniagua, *J. Chem. Phys.* **96**, 1265 (1992).

²⁷A. Aguado, C. Tablero, and M. Paniagua, *Comput. Phys. Commun.* **108**, 259 (1998).

²⁸M. Karplus, R. N. Porter, and R. D. Sharma, *J. Chem. Phys.* **43**, 3259 (1965).

²⁹P. J. Chantry, *J. Chem. Phys.* **55**, 2746 (1971).

³⁰M. E. Weber, J. L. Elkind, and P. B. Armentrout, *J. Chem. Phys.* **84**, 1521 (1986).

³¹J. L. Elkind and P. B. Armentrout, *J. Phys. Chem.* **89**, 5626 (1985).